Title

Tuning the Solvation Structure in Aqueous Zinc Batteries to Maximize Zn-Ion Intercalation and Optimize Dendrite-Free Zinc Plating

Journal

ACS Energy Letters, 7(1)

ISSN

2380-8195

Authors

Li, Chang
Kingsbury, Ryan
Zhou, Laidong
et al.

Publication Date

2022-01-14

DOI

10.1021/acsenergylett.1c02514

Tuning the Solvation Structure in Aqueous Zinc Batteries to Maximize Zn-Ion Intercalation and Optimize Dendrite-Free Zinc Plating

Chang Li,[a, b] Ryan Kingsbury,[c] Laidong Zhou,[a, b] Abhinandan Shyamsunder,[a, b] Kristin A. Persson[b, d, e] and Linda F. Nazar*[a, b]

[a] Department of Chemistry and the Waterloo Institute for Nanotechnology, University of Waterloo, Ontario N2L 3G1, Canada

[b] Joint Center of Energy Storage Research, Argonne National Laboratory, Lemont, Illinois 60439, United States

[c] Energy Storage and Distributed Resources Division, Lawrence Berkeley National Laboratory, 1 Cyclotron Road, Berkeley, California 94720, United States

[d] Molecular Foundry, Lawrence Berkeley National Laboratory, 1 Cyclotron Road, Berkeley, California 94720, United States

[e] Department of Materials Science and Engineering, UC Berkeley, Berkeley, CA 94720

Corresponding Author

* Email: lfnazar@uwaterloo.ca

ABSTRACT: Aqueous zinc batteries are recognized to suffer from H^+/Zn^{2+} co-insertion in the cathode, but few approaches have been reported to suppress deleterious H^+ intercalation. Herein, we realize this goal by tuning the solvation structure, using $LiV_2(PO_4)_3$ (LVP) as a model cathode. Phase conversion of LVP induced by H^+ intercalation is observed in 4 m $Zn(OTf)_2$ whereas dominant Zn^{2+} insertion is confirmed in $ZnCl_2$ water-in-salt electrolyte (WiSE). This disparity is ascribed to the complete absence of free water and the strong Zn^{2+}-H_2O interaction in the latter that interrupts the H_2O hydrogen bonding network, thus suppressing H^+ intercalation. Based on this strategy, a novel PEG-based hybrid electrolyte is designed to replace the corrosive $ZnCl_2$ WiSE. This system exhibits an optimized Zn^{2+} solvation sheath with a similar low free water content, showing not only much better suppression of H^+ intercalation but also highly reversible Zn plating/stripping with a CE of ~99.7% over 150 cycles.

TOC GRAPHIC

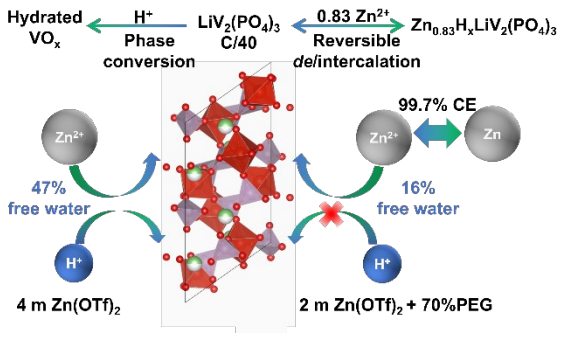

Owing to the high electrodeposition potential of Zn^{2+} (~-0.76V *vs.* SHE), the high theoretical volumetric capacity of the Zn anode (5,850 mAh mL^{-1}) and the advantages of low-cost, high-safety, and eco-friendly operation, aqueous zinc metal batteries (AZMBs) are becoming one of the most attractive technologies for large-scale stationary energy storage.[1, 2, 3] Much work has focussed on developing cathode materials for AZMBs including MnO_2,[4] $Zn_{0.25}V_2O_5 \cdot nH_2O$,[5] along with many others. However, recent studies have found that the high electrochemical capacity of these metal oxides is not solely due to Zn^{2+} insertion/extraction, but largely relies on H^+ (de)intercalation.[6, 7, 8, 9, 10, 11] Proton intercalation results in the formation of layered double-hydroxide salts (LDH, for example, $Zn_4SO_4(OH)_6 \cdot 5H_2O$) on the surface of metal oxides,[8, 9, 10] which aids the reversible and stable operation of metal oxides due to its unique buffering mechanism.[8] On the other hand, the LDH forms an insulating layer on the oxide surface that detaches from the electrode over time, leading to loss of active material. Proton intercalation has now been generally accepted as a common phenomenon for metal oxides in AZMBs.

Studies involving polyanion compounds similarly showed that either H^+ (or Na^+) insertion occurs along with Zn^{2+} intercalation.[12, 13, 14] For example, by analysing the differential capacity curves (dQ/dV) of layered $VOPO_4 \cdot xH_2O$ cathode in different electrolytes, Sun *et al.* found that H^+ intercalation played a dominant role in an electrolyte comprised of 5 m $ZnCl_2$/0.8 m H_3PO_4.[13] Not surprisingly, on increasing the concentration of $ZnCl_2$ to 10 - 13 m, Zn^{2+} was suggested to dominate the intercalation process based on the higher peak intensity of the Zn contribution in the dQ/dV curve. The factors responsible for Zn^{2+} vs. H^+ intercalation (aside from concentration) were not investigated in this study, however. Monoclinic $LiV_2(PO_4)_3$ was reported to be a superior host for AZMBs, and can be cycled at an exceptionally high rate of 60 C.[15] As the high charge density of Zn^{2+} would likely result in limits to solid-state diffusion at this current density and significant structural distortion in monoclinic $V_2(PO_4)_3$,[16] a fundamentally different mechanism based on H^+ intercalation rather than exclusive Zn^{2+} insertion has been proposed to account for this high-rate performance.[11] Recently, an approach to favor Zn^{2+} intercalation was reported for a VPO_4F host lattice based on a hybrid electrolyte (water + propylene carbonate); however proton intercalation still could not be fully suppressed. A multiphase mixture with

overall composition of $Zn_{0.3}H_yVPO_4F$ was formed on discharge, but the implicit existence of a more highly zincated phase could not be quantified.[14]

Herein, we demonstrate that solvation-structure engineering of aqueous Zn electrolytes (AZEs) is an effective method to suppress H^+ intercalation and realize dominant Zn^{2+} intercalation. To establish proof-of-concept, we chose $LiV_2(PO_4)_3$ (LVP) as the platform for the cathode and compared its electrochemistry in two previously reported electrolytes, 4 m (molality, mol/kg) $Zn(OTf)_2$ and 29 m $ZnCl_2$ "water-in-salt" electrolytes (WiSE), as well as a newly designed hybrid electrolyte developed by incorporating polyethylene glycol 400 (PEG 400) and water as a co-solvent with $Zn(OTf)_2$ as the salt. Importantly, we explore the H-bonding network, free water fraction, Zn^{2+}-solvation structure and their roles in the Zn^{2+} vs. H^+ intercalation in all three electrolyte systems, using experimental and computational methods to understand why the PEG-based hybrid electrolyte exhibits the least H^+ intercalation and the most dominant Zn^{2+} intercalation.

The synthesized $Li_3V_2(PO_4)_3$ (Li_3VP) - carbon composite consists of approximately 1 μm aggregate crystallites that are enclosed by conductive carbon (**Figure S1).** ≈ 8.75% carbon content was confirmed by thermogravimetric analysis (TGA), as shown in **Figure S2**. $LiV_2(PO_4)_3$ (LVP) electrodes were prepared by charging Li_3VP electrodes to 1.85 V (vs. Zn^{2+}/Zn) in 4 m $Zn(OTf)_2$, where two Li^+ per formula unit of Li_3VP was successfully extracted. Rietveld refinement of the powder X-ray diffraction (XRD) pattern indicates that all LVP reflections are well indexed to a monoclinic LVP phase with a space group of $P2_1/c$. A unit cell volume contraction of 7.3% upon two Li^+-ion extraction is in close accord with the reported value (**Table S1, 2**).[17]

The electrochemistry of LVP in 4 m $Zn(OTf)_2$ was compared to 29 m $ZnCl_2$ WiSE electrolytes at a 1 C rate (discharge/charge of 1 Zn^{2+} in one hour). Very different electrochemical behavior was observed. As shown in **Figure 1a**, in 4 m $Zn(OTf)_2$ a new discharge plateau below 0.5 V accompanies the increase in capacity and becomes more dominant as the cycle number rises, suggesting a phase conversion process (**Figure 1b**). That process is especially evident in the differential capacity curve (**Figure S3a**). The new lower-voltage plateau was also identified by Wang et al in a spray-dried LVP cathode,[15] but its origin was not disclosed. It should be noted that this low-voltage discharge plateau (~0.5 V vs Zn) is also seen in VO_x-based cathode

materials, indicating H^+ intercalation and the formation of LDHs.[8, 9, 10] In contrast, no lower-voltage plateau was observed in $ZnCl_2$ WiSE, only a minor activation-like process (**Figure 1c, d and S3b**). Strikingly different from the high maximum capacity of 200 mAh g^{-1} exhibited in 4 m $Zn(OTf)_2$, a more realistic discharge capacity of about 90 mAh g^{-1} was recorded at the 60th cycle in $ZnCl_2$ WiSE after the initial activation process. LVP also shows poor cycling stability in 4 m $Zn(OTf)_2$ with only 61% capacity retained after cycling at 1 C for 200 cycles (**Figure 1b**), whereas very good cycling stability with a high capacity retention of about 88% in $ZnCl_2$ WiSE was observed at the same rate for 500 cycles (**Figure 1d**). Such contrasting electrochemistry is also exhibited at higher current densities, as shown in **Figure S4**.

The abnormal electrochemistry observed in 4 m $Zn(OTf)_2$ can be attributed to the decomposition of LVP and the formation of hydrated vanadium oxides (VO_x) phases based on our X-ray diffraction (XRD) studies. The XRD patterns in **Figure 2a** show that monoclinic LVP gradually disappears in 4 m $Zn(OTf)_2$ as the cycle number increases. Simultaneously, two new reflections assigned to hydrated VO_x phases appear, and finally become the major components of the active material (**Figure S5**). The morphology of the LVP electrodes during this phase conversion process was determined by SEM (**Figure 2b**). The well-crystallized particles gradually decompose and exhibit severe loss of crystallinity on cycling. EDX mapping also reveals a gradually decreasing P:V ratio (**Figure S6a**), further supporting the formation of hydrated VO_x phases. In contrast, the structure of LVP was better maintained in $ZnCl_2$ WiSE as cycling progressed (**Figure 2a**), although two small new peaks corresponding to hydrated VO_x appear over a period of 20 cycles. **Figure 2b** and **S6b** shows that the morphology and P:V ratio of LVP electrodes only change slightly in $ZnCl_2$ WiSE, where clear and distinguishable crystalline particles are preserved upon cycling.

To explore whether hydrated VO_x phases result from vanadium dissolution of LVP or H^+ uptake, LVP electrodes were soaked in 4 m $Zn(OTf)_2$, $ZnCl_2$ WiSE, and with the addition of 0.2 m H_3PO_4 to both electrolytes. **Figure 2c** shows the XRD patterns of LVP electrodes that were soaked in the above four electrolytes for 24 hours. The intensity and position of the LVP reflections remain unchanged in 4 m $Zn(OTf)_2$, indicating insignificant vanadium dissolution. However, a major change in the XRD pattern was observed for the electrode soaked in $ZnCl_2$ WiSE for 24 hours, probably caused by ion-exchange of Li^+ for Zn^{2+} owing to their similar ionic

radius and the ultra-high Zn concentration. With the addition of 0.2 m H_3PO_4, this ion exchange process is partially suppressed. While the LVP phase completely disappears in 4 m $Zn(OTf)_2$ + 0.2 m H_3PO_4, two new distinct peaks of hydrated VO_x appear. This pattern is almost the same as fully charged LVP after 20 cycles at C/5 in 4 m $Zn(OTf)_2$ (**Figure S7**), suggesting H^+ uptake is responsible for generating these hydrated VO_x phases.

Dominant Zn^{2+} intercalation of LVP in $ZnCl_2$ WiSE was confirmed by Rietveld refinement of the XRD pattern of fully discharged LVP (at a C/40 rate). As shown in **Figure 3a** and **Table S3**, two independent phases with different amounts of intercalated Zn^{2+} coexist: 59 wt% of a Zn-rich phase ($Zn_{0.81}LiV_2(PO_4)_3$) and 41 wt% of a Zn-deficient phase ($Zn_{0.33}LiV_2(PO_4)_3$). The average fraction of inserted Zn^{2+} was 0.61 per formula unit, corresponding to an electrochemical capacity of 81 mAh g^{-1}. While EDX also shows that around 0.60 Zn^{2+} has intercalated into the lattice (**Figure S8**), the actual discharge capacity is 115 mAh g^{-1} ($\approx$ 0.85 Zn^{2+}, **Figure S9**). The difference of 34 mAh g^{-1} we ascribe to H^+ co-intercalation. Thus, over 70% of the capacity can be attributed to Zn^{2+} intercalation in the LVP lattice. This value is much higher than that reported (< 30%) for V_3O_7,[8] $Ca_{0.34}V_2O_5 \cdot 1.16H_2O$[9] and VPO_4F[18]. The (de)intercalation of Zn^{2+} into LVP was also confirmed by an *ex-situ* XRD study conducted at C/5 on the 2nd cycle (**Figure 3b, c**). With the increasing fraction of intercalated Zn^{2+}, peaks continuously merge and shift to lower angle. During Zn^{2+} *de*intercalation, exactly the converse process was observed, with gradual peak separation and shift to higher angles. This demonstrates the good structural reversibility of LVP as a host for Zn^{2+} insertion/extraction.

The electrochemistry observed for LVP in 4 m $Zn(OTf)_2$ can be ascribed to the decomposition of active materials induced by H^+ intercalation, which likely produces hydrated vanadium oxides as discussed above. This H^+ intercalation process can be largely suppressed by using $ZnCl_2$ WiSE, resulting in dominant and reversible Zn^{2+}-(de)intercalation electrochemistry. Suppression of H^+ intercalation is due to an interrupted H_2O hydrogen bonding network and the existence of only a small fraction of free water molecules in $ZnCl_2$-WiSE as we show below via molecular dynamics (MD) simulations. A systematic study on a similar $ZnCl_2$-WiSE has been carried out by Ji *et al.*[19, 20] FTIR spectroscopy revealed a decreased O-H symmetric stretch (3200 cm^{-1}) and an increased asymmetric stretch (3400 cm^{-1}) on increasing the concentration of $ZnCl_2$ from 5 m to 30 m, suggestive of a strong Zn^{2+}-water interaction that triggers interruption of H_2O

hydrogen bonding network.[19] Furthermore, their MD simulations show that the number of uncoordinated free water molecules in the electrolyte significantly decreases from 10 m $ZnCl_2$ to 30 m $ZnCl_2$.[20]

Nonetheless, while $ZnCl_2$ is low-cost, it is also corrosive at high concentrations. As an alternative approach to reducing H_2O activity, we designed a novel hybrid AZE by using a high concentration of polyethylene glycol 400 (PEG 400) as a crowding agent to form a PEG/H_2O co-solvent. Increased PEG content in 2 m $Zn(OTf)_2$ ($\approx$ 2.2 M) lowers the conductivity and increases the viscosity as expected (**Figure S10**). Nonetheless, σ_i is still 0.7 mS cm^{-1} even at 70 wt% PEG (denoted as 70PEG, see **Methods**), comparable to that of $ZnCl_2$-WiSE.[19] FTIR spectra suggests a strengthened O-H bond owing to the strong H-bonding network between PEG and H_2O (**Figure S11**), which is anticipated to be less favorable to cleavage at the cathode interface in an electrochemical cell.

We propose that H^+ intercalation at the cathode interface can be effectively suppressed owing to this decreased H_2O activity. Indeed, analysis of the Zn^{2+} solvation structure obtained from MD simulations of the bulk electrolyte shows that the Zn^{2+}- H_2O coordination number in 70PEG (2.3) is lower than in 4 m $Zn(OTf)_2$ (3.3, **Figure 4a, S12**), reducing the amount of water available to react at the cathode surface. The Zn^{2+}-H_2O coordination distance is similar in all three electrolytes (**Figure S13**), indicating that the strong Zn^{2+}-H_2O interactions previously observed in $ZnCl_2$ WiSE are operative in 70PEG as well.

Further analysis of our simulations reveals that the fraction of free water is only 16% in 70PEG, compared to 47% in 4 m $Zn(OTf)_2$ and 0% in $ZnCl_2$-WISE (**Figure 4c, Table S4**), presumably resulting in very low water activity. Examination of the structure of the 70PEG shows that PEG400 molecules aggregate to form PEG-rich regions which absorb water but exclude ions (**Figure 4b, d, S14**). This finding is consistent with experimental studies, which have shown that PEG aggregates in aqueous solution, forming internally-hydrated helical structures that result from the balance of hydrophobic and hydrophilic moieties on the molecule.[21] In 70PEG, this internal hydration reduces the free water content and hinders H_2O molecules from transporting to the cathode interface. Thus, we attribute the reduced H^+ intercalation in $ZnCl_2$-WISE and 70PEG to the low availability and reactivity of water molecules.

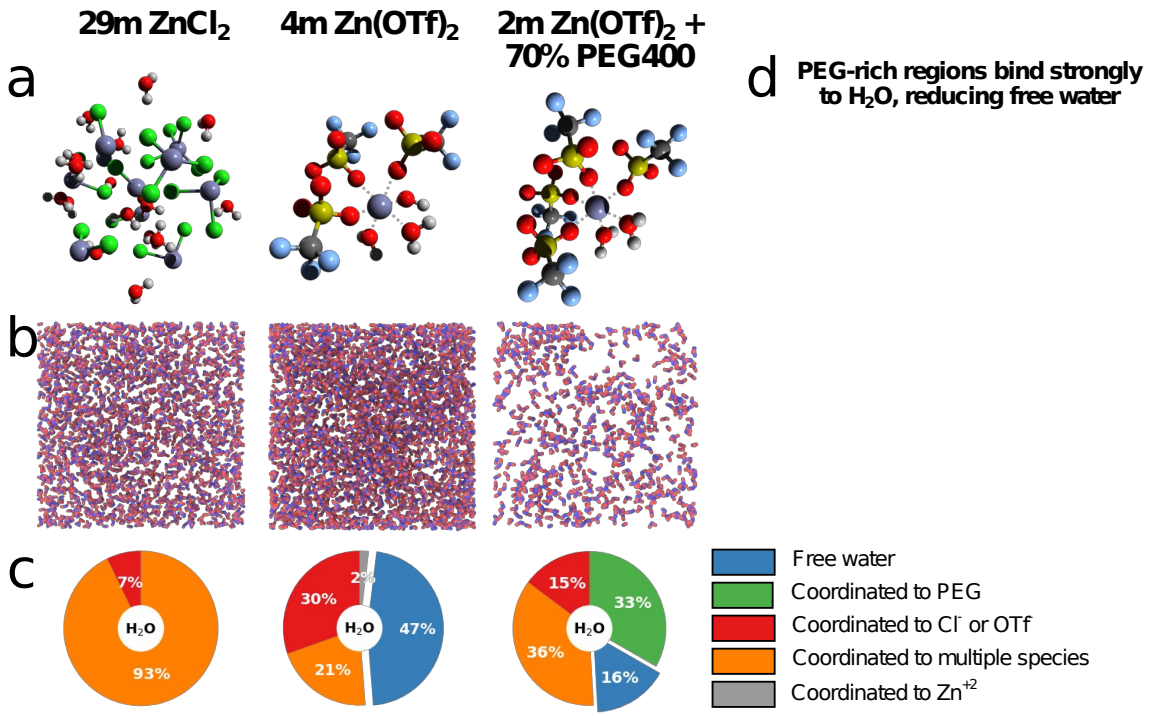

Figure 4. Electrolyte structure in 29m $ZnCl_2$, 4m $Zn(OTf)_2$, and 70PEG electrolytes. (a) Typical Zn^{2+} solvation structures. 29m $ZnCl_2$ WiSE resembles a disordered crystal due to the relative scarcity of water molecules. Zn^{2+} is most commonly coordinated to 3 OTf^- and 3 H_2O in 4m $Zn(OTf)_2$, whereas in 70PEG the solvation shell typically comprises 4 OTf^- and 2 H_2O. (b) Simulation snapshots showing only the water molecules. (c) Distribution of water populations. (d) Water molecules absorbed into the PEG-rich region of the 70PEG electrolyte.

Proof of concept was realized by evaluating Zn plating/stripping behavior for the hybrid AZE in Ti || Zn asymmetric cells, where a very high coulombic efficiency of around 99.7% is achieved for 70PEG at a current density of 1 mA cm^{-2} (1 mAh cm^{-2} capacity), as shown in **Figure 5a, b**. In contrast, 0PEG cells suffer from serious dendrite formation under the same operating conditions and failed after three cycles (**Figure S15**). A Zn || Zn symmetric cell with 70PEG also functions steadily with a capacity of 1 mAh cm^{-2} over more than 1800 hours (> 450 cycles), with a denser and more oriented Zn deposition morphology (**Figure S16** and **S17**). Such dendrite-free Zn plating/stripping is consistent with previous work based on a very low weight ratio of PEG or PEO (<1 wt%) in water, where the adsorption of PEG polymer on the electrode surface was proposed to result in more uniform Zn deposition.[22, 23, 24, 25] In addition, an expanded electrochemical stability window of 2.75 V in 70PEG from 2.32 V in 0PEG can be obtained owing to the reduced water activity (**Figure S18**).

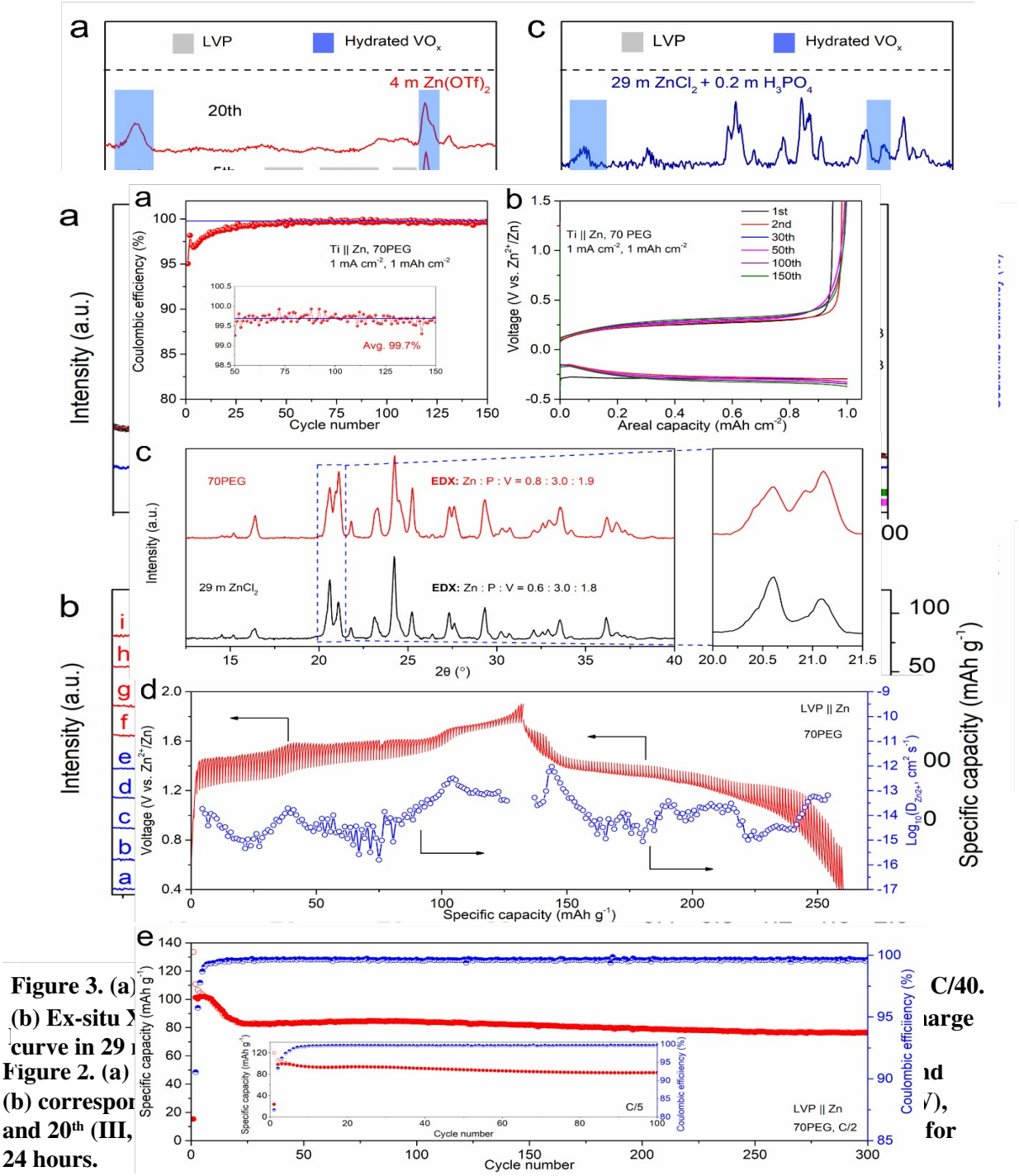

Figure 3. (a) C/40. (b) Ex-situ X arge curve in 29 m

Figure 2. (a) nd (b) correspon V), and 20th (III, for 24 hours.

Figure 5. (a) CE evolution over 150 cycles in 70PEG of Ti || Zn asymmetric cell at 1 mA cm^{-2} for 1 mAh cm^{-2} (Inset = magnified view from 50th to 150th cycles) and (b) corresponding charge-discharge curves. (c) XRD patterns of 2nd fully discharged LVP electrodes in 29 m ZnCl$_2$ and 70PEG at C/40 with corresponding EDX ratios of Zn, P and V. (d) GITT profiles and resulting diffusion coefficient data for LVP in 70PEG at C/40; cells were first discharged prior to charge. (e) Capacity retention of LVP in 70PEG at C/2 and C/5 (inset)

The 70PEG electrolyte is as efficient for suppressing H^+ intercalation as $ZnCl_2$ WiSE in LVP || Zn full cells (**Figure 5c-d**). Compared to the 2nd discharge capacity of 115 mAh g^{-1} (≈ 0.85 Zn^{2+}) in $ZnCl_2$ WiSE, a similar capacity of 112 mAh g^{-1} (≈ 0.82 Zn^{2+}) is obtained at C/40 in 70PEG (**Figure S19**). Analysis of the electrode by EDX shows a composition of 0.83 Zn^{2+} per formula unit, suggesting almost all the capacity is contributed by Zn^{2+} intercalation (compared with only 70% in $ZnCl_2$ WiSE). XRD patterns of these two discharged samples are quite similar (**Figure 5c**), however, the presence of at least three zincated phases lead to a poor Rietveld fit owing to the significant overlap of peaks in these similar structures. Galvanostatic intermittent titration technique (GITT) studies in LVP/70PEG (**Figure 5d**) yielded an average diffusion coefficient of ~10^{-13} - 10^{-16} cm^2 s^{-1} that is about 10^2-10^3 lower than previously reported, presumably owing to the lack of significant contribution from H^+ ion diffusion.[15] Protons are anticipated to be much more mobile due to their small ionic radius and monovalent property. However, direct comparison with LVP/4 m $Zn(OTf)_2$ could not be obtained due to severe phase transformation resulting from very high degrees of proton intercalation at such a low rate of C/40, where endless discharging was observed (**Figure S20**). Long-term Zn^{2+} cycling behavior of LVP in PEG was also evaluated at higher rates (**Figure 5e**). After an initial activation process, LVP can be cycled steadily with capacity retention of 83.5% after 100 cycles at C/5 and 74.5% after 300 cycles at C/2. Compared to the evolution of the charge/discharge curve profiles upon cycling cells in 4 m $Zn(OTf)_2$, only a slight change can be observed in 70PEG (**Figure S21**). The absence of a voltage plateau below 0.5 V also indicates the suppression of H^+ intercalation.

In summary, our studies of 4 m $Zn(OTf)_2$, 29 m $ZnCl_2$ WiSE and 2 m $Zn(OTf)_2$ PEG-based hybrid electrolyte on Zn^{2+} vs. H^+ insertion/extraction of an LVP cathode, reveal the effect of solvation structure and H_2O hydrogen bonding network on H^+ intercalation. Proton co-intercalation verified in 4 m $Zn(OTf)_2$ is suppressed in $ZnCl_2$ WiSE by the interrupted hydrogen bonding network induced by a strong Zn^{2+}-H_2O interaction and few free H_2O molecules, resulting in dominant Zn^{2+} intercalation that is confirmed quantitatively by Rietveld refinement and EDX. A reduced free water content and further optimized solvation structure was identified in a 2 m $Zn(OTf)_2$ PEG-based hybrid electrolyte, where 70PEG shows excellent reversibility and stability for Zn plating/stripping and much better suppression of H^+ intercalation due to the strong interaction between PEG and H_2O. The excellent ultra low-rate electrochemical

performance (C/40) of LVP in 70PEG also suggests the hybrid electrolyte outperforms the conventional low-concentration aqueous electrolyte to realize dominant Zn^{2+} intercalation. Our work demonstrates that tuning the solvation structure and building strong interactions between H_2O and PEG to interrupt the H_2O hydrogen bonding network is an effective strategy to suppress detrimental H^+ intercalation, maximize Zn^{2+} intercalation and achieve highly reversible Zn utilization.

ASSOCIATED CONTENT

Supporting Information.

This material is available free of charge via the Internet at http://pubs.acs.org.

Experimental methods, electrochemical measurements, Rietveld refinements and lattice parameters.

AUTHOR INFORMATION

Corresponding Author

* Email: lfnazar@uwaterloo.ca

ORCID

Linda F. Nazar: 0000-0002-3314-8197

Chang Li: 0000-0001-5420-3856

Author Contributions

C.L. and L.F.N. designed this study. C.L. synthesized the materials, carried out the characterization and all the electrochemical measurements. R.K. and K.A.P. performed molecular dynamics simulations. L.Z. helped with the Rietveld refinements. A.S. helped to perform the GITT measurement. C.L. and L.F.N. wrote the manuscript with contributions from R.K. and K.A.P.

Notes

The authors declare no competing financial interest.

ACKNOWLEDGMENTS

This work was financially supported by the Joint Centre for Energy Storage Research, an Energy Innovation Hub funded by the US. Department of Energy, Office of Science, Basic Energy Sciences. We would like to thank C.Y. Kwok (University of Waterloo) for help with acquiring the SEM data. L.F.N also acknowledges NSERC for platform support through the Discovery Grant and Canada Research Chair programs. The authors gratefully acknowledge Orion Cohen, Alex Epstein, Kara Fong, and Tingzheng Hou (University of California, Berkeley) for helpful discussions and assistance setting up the molecular dynamics simulations.

REFERENCES

[1]() Liu, Z.; Huang, Y.; Huang, Y.; Yang, Q.; Li, X.; Huang, Z.; Zhi, C. Voltage Issue of Aqueous Rechargeable Metal-Ion Batteries. *Chem. Soc. Rev.* **2020**, *49*, 180-232.

[2]() Demir-Cakan, R.; Rosa Palacin, M.; Croguennec, L. Rechargeable Aqueous Electrolyte Batteries: From Univalent to Multivalent Cation Chemistry. *J. Mater. Chem. A* **2019**, *7* (36), 20519–20539.

[3]() Blanc, L. E.; Kundu, D.; Nazar, L. F. Scientific Challenges for the Implementation of Zn-Ion Batteries. *Joule* **2020**, *4*, 771-799.

[4]() Pan, H.; Shao, Y.; Yan, P.; Cheng, Y.; Han, K. S.; Nie, Z.; Wang, C.; Yang, J.; Li, X.; Bhattacharya, P.; Mueller, K. T.; Liu, J. Reversible Aqueous Zinc/Manganese Oxide Energy Storage from Conversion Reactions. *Nature Energy* **2016**, *1* (5), 16039.

[5]() Kundu, D.; Adams, B. D.; Duffort, V.; Vajargah, S. H.; Nazar, L. F. A High-Capacity and Long-Life Aqueous Rechargeable Zinc Battery Using a Metal Oxide Intercalation Cathode. *Nature Energy* **2016**, *1* (10), 16119.

[6]() Sun, W.; Wang, F.; Hou, S.; Yang, C.; Fan, X.; Ma, Z.; Gao, T.; Han, F.; Hu, R.; Zhu, M.; Wang, C. Zn/MnO_2 Battery Chemistry With H^+ and Zn^{2+} Coinsertion. *J. Am. Chem. Soc.* **2017**, *129*, 9775-9778.

[7]() Huang, J.; Wang, Z.; Hou, M.; Dong, X.; Liu, Y.; Wang, Y.; Xia, Y. Polyaniline-Intercalated Manganese Dioxide Nanolayers as a High-Performance Cathode Materials for An Aqueous Zinc-Ion Battery. *Nature Commun.* **2018**, *9*, 2906.

[8]() Oberholzer, P.; Tervoort, E.; Bouzid, A.; Pasquarello, A.; Kundu, D. Oxide versus Nonoxide Cathode Materials for Aqueous Zn Batteries: An Insight into the Charge Storage Mechanism and Consequences Thereof. *ACS Appl. Mater. Interfaces* **2019**, *11* (1), 674–682.

[9]() Liu, X.; Euchner, H.; Zarrabeitia, M.; Gao, X.; Elia, G. A.; Grob, A.; Passerini, S. Operando pH Measurements Decipher H^+/Zn^{2+} Intercalation Chemsitry in High-Performance Aqueous $Zn/\beta\text{-}V_2O_5$ Batteries. *ACS Energy Lett.* **2020**, *5*, 2979-2986.

[10]() Zhang, L.; Rodriguez-Perez, I. A.; Jiang, H.; Zhang, C.; Leonard, D. P.; Guo, Q.; Wang, W.; Han, S.; Wang, L.; Ji, X. $ZnCl_2$ "Water-in-Salt" Electrolyte Transforms the Performance of Vanadium Oxide as a Zn Battery Cathode. *Adv. Funct. Mater.* **2019**, *20*, 1902653.

[11]() Park, M. J.; Asl, H. Y.; Manthiram A. Multivalent-Ion versus Proton Insertion into Battery Electrodes. *ACS Energy Lett.* **2020**, *5*, 2367-2375.

[12]() Ko, J. S.; Paul, P. P.; Wan, G.; Seitzman, N.; DeBlock, R. H.; Dunn, B. S.; Toney, M. F.; Weker, J. N. NASCION $Na_3V_2(PO_4)_3$ Enables Quasi-Two-Stage Na^+ and Zn^{2+} Intercalation for Multivalent Zinc Batteries. *Chem. Mater.* **2020**, *32*, 3028-3035.

[13]() Shi, H.-Y.; Song, Y.; Qin, Z.; Li, C.; Guo, D.; Liu, X.-X.; Sun, X. Inhibiting $VOPO_4{\cdot}xH_2O$ Decomposition and Dissolution in Rechargeable Aqueous Zinc Batteries to Promote Voltage and Capacity Stabilities. *Angew. Chem. Int. Ed.* **2019**, *58* (45), 16057-16061.

[14]() Wang, F.; Blanc, L. E; Li, Q.; Faraone, A.; Ji, X.; Chen-Mayer, H. H.; Paul, R. L.; Dura, J. A.; Hu, E.; Xu, K.; Nazar, L. F.; Wang C. Quantifying and Suppressing Proton Intrcalation to Enable High-Voltage Zn-Ion Batteries. *Adv. Energy Mater.* **2021**, *11*, 2102016.

[15]() Wang, F.; Hu, E.; Sun, W.; Gao, T.; Ji, X.; Fan, X.; Han, F.; Yang, X.-Q.; Xu, K.; Wang, C. A Rechargeable Aqueous Zn^{2+}-Battery with High Power Density and a Long Cycle-Life. *Energy Environ. Sci.* **2018**, *11* (11), 3168–3175.

[16]() Park, M. J.; Asl, H. Y.; Therese, S.; Manthiram, A. Structural Impact of Zn-Insertion into monoclinic $V_2(PO_4)_3$: Implications for Zn-Ion Batteries. *J. Mater. Chem. A.* **2019**, *7*, 7159-7167.

[17]() Yin, S.; Grondey, H.; Strobel, P.; Anne, M.; Nazar, L. F. Electrochemical Property: Structure Relationships in Monoclinic $Li_{3-y}V_2(PO_4)_3$. *J. Am. Chem. Soc.* **2003**, *125*, 10402-10411.

[18]() Asl, H. Y.; Sharma, S.; Manthiram, A. The Critical Effect of Water Content in the Electrolyte on the Reversible Electrochemical Performance of Zn-VPO_4F Cells. *J. Mater. Chem. A.* **2020**, *8*, 8262.

[19]() Zhang, C.; Holoubek, J.; Wu, X.; Daniyar, A.; Zhu, L.; Chen, C.; Leonard, D. P.; Rodriguez-Perez, I. A., Jiang, J.; Fang, C.; Ji, X. A $ZnCl_2$ Water-in Salt Electrolyte for A Reversible Zn Metal Anode. *Chem. Commun.* **2018**, *54*, 14097.

[20]() Zhang, C.; Shin, W.; Zhu, L.; Chen, C.; Neuefeind, J. C.; Xu, Y.; Allec, S. I.; Liu, C.; Wei, Z.; Daniyar, A.; Jiang, J.-X.; Fang, C.; Alex Greaney, P.; Ji, X. The electrolyte comprising more robust water and superhalides transforms Zn-metal anode reversibly and dendrite-free. *Carbon Energy* **2020**, *3*, 1−10.

[21]() Azri, A.; Giamarchi, P.; Grohens, Y.; Olier, R.; Privat, M. Polyethylene Glycol Aggregates in Water Formed through Hydrophobic Helical Structures. *J. Colloid Interface Sci.* **2012**, *379* (1), 14-19.

[22]() Mitha, A.; Yazdi, A. Z.; Ahmed, M.; Chen, P. Surface Adsorption of Polyethylene Glycol to Suppress Dendrite Formation on Zinc Anodes in Rechargeable Aqueous Batteries. *ChemElectroChem* **2018**, *5*, 2409-2418.

[23]() Jin, Y.; Han, K. S.; Shao, Y.; Sushko, M. L.; Xiao J.; Pan, H.; Liu, J. Stabilizing Zinc Anode Reactions by Polyethelene Oxide Polymer in Mild Aqueous Electrolytes. *Adv. Funct. Mater.* **2020**, *30*, 2003932.

[24]() Yan, M.; Xu, C.; Sun, Y.; Pan, H.; Li, H. Manipulating Zn anode reactions through salt anion involving hydrogen bonding network in aqueous electrolytes with PEO additive. *Nano Energy* **2021**, *82*, 105739.

[25]() Yan, M.; Dong, N.; Zhao, X.; Sun, Y.; Pan, H. Tailoring the Stability and Kinetics of Zn Anodes through Trace Organic Polymer Additives in Dilute Aqueous Electrolyte. *ACS Energy Lett.* **2021**, *6*, 3236-3243.